Egypt.J.Chem. **Vol. 62**, No. 8. pp. 1499 - 1517 (2019)

Egyptian Journal of Chemistry
http://ejchem.journals.ekb.eg/

Removal Comparative Study for Cd(II) Ions from Polluted Solutions by Adsorption and Coagulation Techniques Using Moringa Oleifera Seeds

A. A. Swelam[1], Sherif S. S.[2] and A. I. Hafez[1*]
[1]*Faculty of Science, Physical Chemistry Dept. Al Azhar University, Egypt.*
[2]*Medicinal and Aromatic Dept. Horti. Res. Institute, A. R. C., Egypt.*

THE *MORINGA oleifera* seed (MOS) was characterized by pHzpc, Fourier transform infrared spectroscopy (FT-IR), X-ray and scanning electron microscopy (SEM) in order to get an insight of the surface charge, functional groups, and morphology of the biosorbent, respectively. The MOS studies were conducted on Cd (II) with different parameters, such as solution pH, contact time, initial concentration of the pollutant and temperature were examined. Experimental results revealed an increase of the removal percentage of Cd (II) using coagulation compared with adsorption technique with increases of the initial Cd (II) concentration, contact time, pHs and temperatures. The Freundlich isotherm linear equation is better described for the adsorption process and coagulation process for the removal of Cd (II) ions. By Comparing the thermodynamic parameters of Cd (II) removal, such as ΔH, ΔS and ΔG, distinct behaviours were observed, where adsorption process is positive values along all temperatures while coagulation process showed negative values. According to S* value, the adsorbent system is very high while the coagulation system is very low.

Keywords: Moringa Oleifera seeds, Cd (II), Adsorption, Thermodynamics, Coagulation.

Introduction

The challenge of contamination of natural waters by various chemical species continues to be of great concern worldwide especially when the resource is becoming scarce. Heavy metals are amongst the common pollutants detected in several aquatic environments. The metal ions are not bio-degradable and usually bio-accumulate in living organisms tissues [1]. For example nickel (Ni), copper (Cu), zinc (Zn), aluminum (Al), lead (Pb) and Cd (II) (Cd) are by products of heavy industries such as electro-plating, petro-chemical processing, batteries, mining, metallurgical process, brewery, pharmaceuticals, paper and pulp, plastic and paint [2,3]. Several research studies have come up with ways of minimising the adverse effects of these heavy metal ions such as chemical precipitation, coagulation, solvent extraction, electrolysis, membrane separation, and ion-exchange techniques [4]. The majority of these methods require high initial and running costs. In order to reduce the high investments, rigorous research has been carried out to find innovative and cost effective methods. Bio-adsorption has received much attention and has currently become an extensive area of research. This process is very effective and versatile for the removal of heavy metals from industrial effluents at relatively lowest costs.

Coagulation can be considered an important process for industrial wastewater pretreatment since it is quite effective in the removal of suspended solids [5]. Inorganic coagulants and synthetic polymers such as aluminum polychloride, aluminum sulfate, and ferric sulfate are commonly employed [6]. This process consists essentially in chemically and physically destabilizing colloidal/suspended particles. Thus,

*Corresponding author e-mail: a7med_el3med@yahoo.com
Received 22/12/2018; Accepted 7/3/2019
DOI: 10.21608/EJCHEM.2019.6801.1568

the treatment is expected to remove impurities, especially turbidity, toxic substances (organic and inorganic) and colloidal organic matter [7]. Although synthetic coagulants show good performance in the process of destabilizing suspended matter, and have some disadvantages such as the production of large amounts of non-biodegradable sludge and high levels of toxicity [8]. Vegetable coagulants (or biocoagulants), which are biodegradable, non-toxic, and produce very little residual sludge [9], are an alternative to overcome the main disadvantage of coagulation processes (which is the use of synthetic coagulants).

Moringa Oleifera (MO), a plant species that belongs to the family *Moringa ceae* is quite abundant in Brazil. Despite the paucity of studies about the use of *Moringa oleifera* aqueous extract (MOSAE) as a coagulant, some researchers have found that this species is fairly effective in the treatment of several types of wastewaters [10]. On the other hand, considering that the composition of MOAE includes significant amounts of proteins, carbohydrates and lipids and that these substances may remain in the treated wastewater at the end of the coagulation process, the wastewater tends to have a high organic load [11]. Residual organic matter in treated wastewater can be disadvantageous if the water is to be reused, since microorganisms develop easily in these conditions. According to Dey et al. [12], microbial activity in recycled wastewater from water-based paint manufacturing processes decreases the quality and service life of the end product. Therefore, depending on the final destination of treated wastewater, it may be necessary to include other methods that can destroy or decrease residual organic matter (from vegetable coagulant agents).

Vieira et al. [13] showed that MO seeds used as a natural adsorbent have a strong removal efficiency reaching up to 98% for both color and turbidity. While Arnoldsson et al. [14] mentioned the negligible effect of MO seeds as a coagulant on pH, alkalinity or conductivity of water. MO seeds have not only been studied for their coagulating properties but also for their ability to remove heavy metals from aqueous solutions. A study by Nand et al. [15] showed that MO was capable on adsorbing heavy metals more than other seed types. The percentage of removal was 90% for copper, 80% for lead, 60% for Cd (II) and 50% for zinc and chromium.

In this study, Moringa oleifera seed powder (MOS), was used for the removal of Cd (II) by using the adsorption technique compared for coagulation technique from aquatic pollutants (metal pollutant). The MOS was characterized by pH_{pzc}, FT-IR, X-ray and SEM analyses to gain an insight of physico-chemical properties. The experimental conditions were optimized through batch experiments by studying different parameters, viz. effect of contact time, solution pH and initial concentration of the Cd (II) ions. In addition to evaluation of four isotherm models and various thermodynamic parameters

Experimental

Materials

Synthetic solutions were prepared by dissolving a desired amount of Cd (II) acetate (g) of analytical grade in distilled water to obtain stock solution. All the chemicals used were of analytical grade. Distilled water was used throughout the experiments

Source of M. Oleifera seeds

M. Olifera seeds were obtained from Al Qalyobia governorate farms by Medicinal and Aromatic Dept., Horticulture Res. Institute, A.R.C., Egypt during March, 2017. The seeds were identified by the Horticulture Research Institute of Egypt. Seeds de-shelled by hand grounded in a domestic blender and sieved through 0.08mm stainless steel sieve.

Instrumentation

The pH of the solution was determined using a HANNA instruments pH meter (pH 209 models, Portugal). The surface morphology was studied using a Jeol (Tokyo, Japan) JSM 5600 LV. Oxford instruments 6587 EDX micro-analysis detector EDX micro-analysis was made to obtain information on the elemental composition of the sample (Egypt Nanotechnology Center, Cairo University, Shaikh Zayed Campus, B3). A micromeritics (Novatouch LX2, Quanta chrome Instruments, Boynton Beach, Florida, USA (Egypt Nanotechnology Center, Cairo University, Shaikh Zayed Campus, B3 instrument) was used for Brunau-Emmett-Teller (BET) analysis to determine surface area, total pore volume, and average pore size of moringa seed powder. In a BET surface area analysis, a dry sample was evacuated of all gas and cooled to 77 K using liquid nitrogen.

Adsorption experiments

The batch experiment was carried out by sieved powered seeds and weighing 0.666 g. A desired amount of the metal ion solution was added and the mixture was shaken in a mechanical shaker at 100 rpm for a definite period of time until equilibrium was reached and then centrifuge for about 3-5 min. The supernatant solution was analyzed with atomic spectroscopy. The desired pH was adjusted by adding negligible volumes of 0.01 and/or 0.1 mol/L HCl or NaOH solution. The amount of adsorbate adsorbed per unit weight of adsorbent (q_e (mg/g)) was calculated by the following equation:

$$q_e = \frac{(C_0 - C_e)V}{W \times 1000} \quad (1)$$

Where w is the mass of adsorbent, V is the volume of suspension, C_0 (ppm) and C_e (ppm) are the initial and equilibrium concentrations of adsorbates.

Coagulation experiments

One gram of MOS powder was added to 100ml distilled water and stirred 200 rpm for 15 minutes using magnetic stirrer to create active constituents to prepare stoke solution of 1% W/v. All coagulation experiments were carried out in the 100 ml transparent bottles, and the samples were left undisturbed on a flat surface for 72 h to allow for the complete settlement of MOS and the large Cd(II) aggregates. The pH was adjusted by adding negligible volume of 0.1 or 0.01 M HCl and/or NaOH. HCl and NaOH did not affect the coagulation of Cd (II) on MOS with varied pH. The effects of contact time, pH and coagulation temperature on Cd (II) coagulation were investigated. The residual concentration of Cd (II) in supernatant was separated by centrifugation at 1000 rpm for 10 min measured by AAS spectrophotometer. The coagulation of Cd (II) in synthetic water systems was carried out to study the behavior of Cd (II) under natural aqueous solutions. The Cd (II) removal percentage was calculated using Eq. (2):

$$\text{The removal percentage yield (R \%)} = \frac{C_0 - C_e}{C_0} \times 100 \quad (2)$$

Each experimental data point is obtained as the average value of triplicate parallel samples (the resulting error bars (within ±5%) are provided).

Adsorption isotherm of the Cd (II) ions.

Freundlich Adsorption Isotherm:

The Freundlich isotherm [16] is derived by assuming a heterogeneous surface with a non-uniform distribution of heat of sorption over the surface. It can be stated in the linear form as follows:

$$\ln q_e = \ln K_F + \frac{1}{n} \ln C_e \quad (3)$$

Where K_F (mg g^{-1}) and n are isotherm constants indicate the capacity and intensity of the adsorption, respectively.

Langmuir Adsorption Isotherm

The Langmuir equation [17] is represented in the linear form as follows:

$$\frac{C_e}{q_e} = \frac{1}{K_L Q_{max}} + \frac{C_e}{Q_{max}} \quad (4)$$

Where C_e is the equilibrium concentration of adsorbate q_e (ppm), is the amount of soluted sorbate at equilibrium (mg/g), K_L is the Langmuir adsorption constant (L $mmol^{-1}$) and Q_{max} is the theoretical maximum adsorption capacity (mg/g). Langmuir plots $\left(\frac{C_e}{q_e} \; vs. \; C_e\right)$ for adsorption of metal ions onto resins at different temperatures.

For the Langmuir isotherm model, a dimensionless constant (R_L), commonly known as separation factor or equilibrium parameter can be used to describe the favorability of adsorption on the polymer surface by:

$$R_L = \frac{1}{1 + K_L C_0} \quad (5)$$

Where C_0 is the initial metal ions concentration and K_L is the Langmuir equilibrium constant.

The Temkin Isotherm

The Temkin isotherm [18] has been used in the following form:

$$q_e = \left(\frac{RT}{b_T}\right) \ln A_T + \left(\frac{RT}{b_T}\right) \ln C_e \quad (6)$$

Where $B_T = \left(\frac{RT}{b_T}\right)$, B_T is the Temkin constant (J/mol) related to adsorption heat, T is the absolute temperature (K), R is the gas constant (8.314 J/mol K), and A_T is the Temkin isotherm constant (L/g). (B_T) and (A_T) can be calculated from the slopes (b_T) and intercepts $(b_T \ln A_T)$ of the plot of q_e vs. $\ln C_e$.

Dubinin–Radushkevich isotherm model

The linear form of Dubinin and RadushKevich isotherm equation [19] can be expressed as:

$$\ln q_e = \ln(X_{D-R}) - \beta\varepsilon^2 \quad (7)$$

Where X_{D-R} is the theoretical monolayer saturation capacity (mmol g^{-1}), is the Dubinin–Radushkevich model constant ($mol^2\ J^{-2}$). Ɛ is the polanyi potential and is equal to

$$\varepsilon = RT\ln\left(1+\frac{1}{C_e}\right) \quad (8)$$

where R, T and C_e represent the gas constant (8.314 J/mol K), absolute temperature (K) and adsorbate equilibrium concentration (mmol/L), respectively.

The X_{D-R} and β can be calculated from the slopes (–β) and In X_{D-R} intercepts of the plot of $(\ln q_e)$ vs. (ε^2) at different temperatures for metal ions onto the resins.

The value of E_{D-R} is related to the sorption mean free energy (KJ/mol). The relationship is expressed as:

$$E_{D-R} = \frac{1}{\sqrt{-2\beta}} \quad (9)$$

Adsorption thermodynamics.

The sorption data obtained from the above study (i.e. Effect of system temperature of sorption process) was used to calculate the thermodynamic parameters. The calculated Gibbs free energy change (ΔG), enthalpy change (ΔH) and entropy change (ΔS) values for the sorption process of metal ions by the three resins.

The Gibbs free energy change, (ΔG)(kJ/mol) was calculated from the following equation;

$$\Delta G = -RT\ln K_d \quad (10)$$

Where *R* is the universal gas constant (8.314 J mol^{-1} K^{-1}), *T* is the absolute temperature (*K*) and K_d is the distribution coefficient of the adsorbate.

The relation between (ΔG) (kJ mol^{-1}), (ΔH) (kJ mol^{-1}) and (ΔS) (kJ mol^{-1} K^{-1}) can be expressed by the following equation;

$$\Delta G = \Delta H - T\Delta S \quad (11)$$

The van't Hoff equation

$$\ln K_d = \frac{\Delta S}{R} - \frac{\Delta H}{RT} \quad (12)$$

The values ΔH of ΔS and were obtained from the slope $\left(\frac{-\Delta H}{R}\right)$ and intercept $\left(\frac{\Delta S}{R}\right)$ respectively, of the plot of $\ln K_d$ vs. $\frac{1}{T}$.

In order to further support the assertion that physical adsorption is the predominant mechanism, the values of the activation energy (E_a) and sticking probability (S^*) were estimated from the experimental data. They were calculated using a modified Arrhenius type equation related to surface coverage (θ) [20] as expressed in equations:

$$\theta = 1 - \frac{C_e}{C_0} \quad (13)$$

Where C_0 and C_e are the initial and equilibrium metal ion concentrations, respectively

$$S^* = (1-\theta)\exp\left(\frac{E_a}{RT}\right) \quad (14)$$

The sticking probability, *S**, is a function of the adsorbate/adsorbent system under consideration and is dependent on the temperature of the system.

The combination of Eqs. (13) and (14) gives the equation (15):

$$\ln\frac{C_e}{C_0} = \ln S^* + \frac{E_a}{RT} \quad (15)$$

The values of E_a and *S** were obtained from the slope $\left(\frac{E_a}{R}\right)$ and intercept In*S**, respectively, of the plot of $\ln\frac{C_e}{C_0}$ vs. $\frac{1}{T}$.

Results and Discussion

Characterization

Fourier transforms infrared (FT-IR) spectroscopy

It is very crucial to elucidate the functional groups in order to understand the interaction between the protein and the metal ion. The Fourier Transform Infrared (FT-IR) spectra (Fig. 1) of MOS (unloaded) and metal-loaded MOS were recorded at 400–4000 cm^{-1} range using an FT-IR to investigate the functional groups present on the bio-sorbent surface.

The bands in approximately 2924.8 $cm^{-1}$and 2854.1 cm^{-1} were assigned to the symmetric and asymmetric stretching of group C-H-CH_2 present in fatty acids [21]. The spectra showed two strong absorption bands at 1657.5 $cm^{-1}$and 1543.7 cm^{-1} characteristics of amide I and II respectively, which confirms the structure of the protein present in moringa seeds and in approximately 1114.4 cm^{-1}, concerning the presence of polysaccharides [22]. Thus, in general, the FT-IR's spectra of MOS (showed the presence of various functional groups that indicating their complex nature) The peak at 1746 cm^{-1} in the MOS spectrum shows the carbonyl (C=O) stretching vibration of the carboxyl groups of lignin in the MO [23]. The broad peak in spectra at 3313.1 cm^{-1} is indicative of strong O-H (H-bonded) stretching [24]. It can be observed from Fig. 1 that referring to MOS as the substrate for adsorption, the peaks in both

the spectra obtained before and after adsorption displayed characteristic bands at 870.4, 789.6 and 461.8 cm^{-1} for the raw MOS, bands at 851.2, 582.2 and 462.3 cm^{-1} for adsorption of Cd (II) ions (Fig. 1) which can be attributed to Si-O stretching modes and Si-O-Si bending modes including distortion modes associated primarily with oxygen and silica atoms respectively [25] and bands at 1096.9, 852.3 and 463.1 cm^{-1} for adsorption of Cd (II) ions.

In this work, it was observed that the *Moringa olefira* seed has amide, amine, carboxylic acid, hydroxyl and other functional groups, which possibly confirmed the presence of most of the necessary functionalities in the current study. A similar type of moringa seed spectra has also been reported by other scientists, during different research findings [26-28].

By Comparison the FT-IR spectra of the MOS before and after adsorption of the metal ions revealed that, after adsorption of Cd (II), the peaks were shifted significantly or not changed. The shifting in the peak positions and intensity in the spectra, after Cd (II) adsorption, signifies the participation of those specific groups in sorption process. So the functional groups like O-H, C-N, N-H and C-O are possibly playing their role in sorption phenomenon by developing some electrostatic-forces [24] or complexation and etc. [29] between the functional groups on bio-sorbent surfaces and the metal ions.

In addition, there is a need to perform structural studies under the conditions in which protein actually operates (i.e. generally in solution). Thus, further investigations are necessary to study the infrared spectra of the adsorbent protein in aqueous solution. The change in the positions of the groups confirmed their role in the ion binding to the MOS surface [30,31].

XRD diffraction of Moringa oleifera seeds

A powerful tool for showing the crystalline and amorphous region is XRD spectroscopy. The XRD patterns of MOS, MOS-Cd systems. Figure 2 shows the X-ray diffraction pattern of *Moringa stenopetala* seed powder. According to Abudikarim et al**.** [32], around 69% weight of the seeds composed of high amount of oil and protein. Due to the high composition of protein and oil, the X-ray pattern showed a broad band around $2\Theta = 20°$ for the seed powder which is attributed to the predominance of amorphous nature of the material. The presence of this peak is probably associated with diffraction of the constituent protein surrounding the other components that have a more amorphous or semi crystalline nature [33]. According to Araújo et al. 2013 and Maria et al., [34,35], the amorphous nature of the adsorbent suggests that the adsorbate can more easily penetrate the surface of the adsorbent, thus favoring the adsorption process.

A noticeable change in the X-ray diffraction (XRD) peak positions is observed due to the addition of Cd (II) ions. Therefore, it is concluded that the incorporation of the ions in the MOS

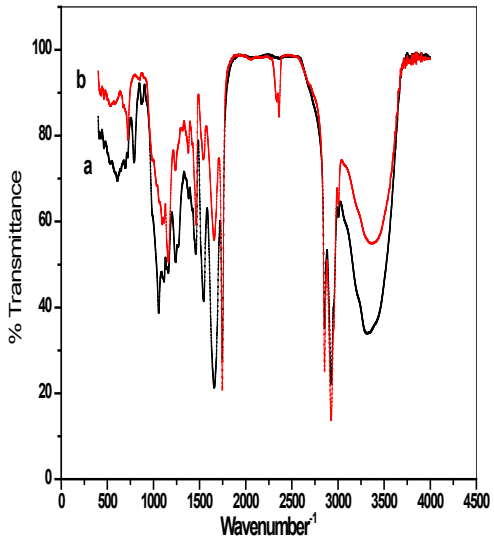

Fig. 1. FT-IR diffraction of Moringa oleifera seed before (a) and after (b) Cd(II) adsorption

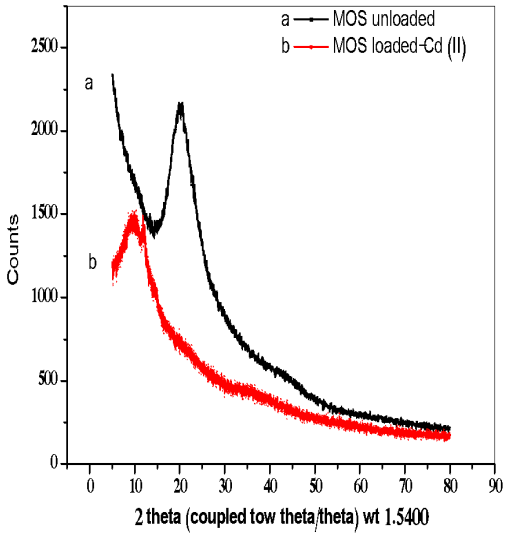

Fig. 2. XRD of Moringa oleifera seed before (a) and after (b) Cd(II) adsorption.

affects the amorphous surface of the MOS, thus increasing crystalline structure. This is due to the fact that the replacement of protons of hydroxyl and carboxylic groups presented on the MOS surface, thus the adsorption of these ions was partially via ion exchange mechanism**.** Then, this explains the formation of new peaks, disappearance of others and band shifts observed on the water-soluble protein powder after removal.

A scanning electron microscope (SEM)

Figure 3a shows SEM images of the Moringa oleifera seeds used to analyze the morphologies of the studied adsorbent. Figure 3a shows that the material formed by MOS is villous. It can be speculated that the villus plays an important role in the adsorption process [36]. It is observed also that, the material exhibit a heterogeneous and relatively porous matrix. The available spaces facilitate the adsorption process because they provide a high internal surface area. The same conclusion was reported by Araújo et al. [21]. The author also explains that this structure facilitates the ionic adsorption processes due to the interstices and, more importantly, the presence of the protein component of the seed. The porous nature of this material can also be observed in the data obtained with the BET analysis. The results also indicate that, there was a layer covering the surfaces of the Moringa oleifera seed, possibly Cd (II) (Fig. 3b). A similar type of other adsorbent spectra has also been reported by other scientists, during different research findings [37,38].

To further confirmation the role of the localized elemental information of MOS, the EDX study was determined, which presented the important elements of the MOS adsorbent (Fig. 4a). The oxygen, nitrogen and silicon element occurs at the surface, which are favorable for the adsorption of heavy metal ions. The presence of C is also associated with the high protein content in MO seeds [39] which contributes to the efficiency of this material in the adsorption process. Based on the results of Fig. 4b, it can be found that the the oxygen atoms (O) were significantly reduced after adsorption while the Cd (II) ions peaks were appeared. The reduction of oxygen atoms (O) may be contribution of ion exchange reaction with heavy metal ions Cd (II) in the adsorption process. Consequently, it can be summarized that the surface oxygen-containing functional groups and other metal ions of adsorbent have a significant role in the adsorption process.

Adsorption process

Effect of initial concentration

Effect of the initial concentration of Cd (II) ions on adsorption capacity was studied in the range of 236 to 662 ppm at pH ~7 using 0.666 mg of MOS adsorbent (Fig. 5). That the adsorption capacity increased significantly from 8.11 to 22.15 ppm as the initial Cd (II) ions concentration increased from 236 ppm to 662 ppm. The observed behaviour can be explained on the basis of the availability of the active binding sites on the fixed dosage of the adsorbent. At lower concentration, Cd (II) ions in the solution would occupy the sufficient binding sites and result in the higher adsorption. However at higher concentration saturation of the limited binding sites occurs and more Cd (II) ions will remain unadsorbed which results in lower adsorption [40].

The higher the initial concentration of Cd (II), the larger was the equilibrium adsorption capacities of Cd (II) on MOS biosorbent. (Fig. 5)The results can ascribed to the fact that initial

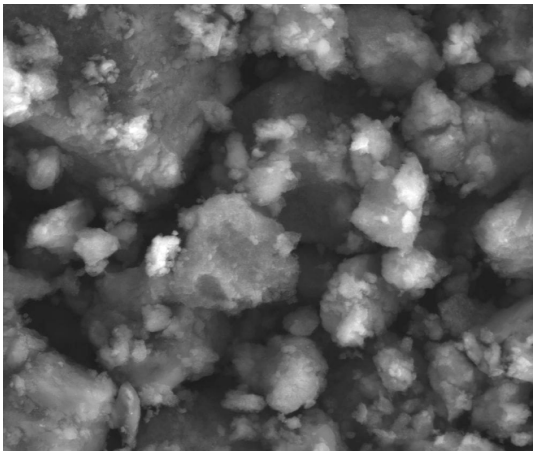

Fig. 3a. SEM scanning images of raw MOS.

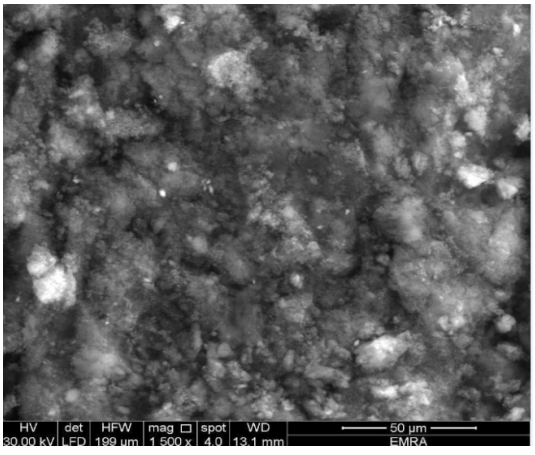

Fig. 3b.SEM scanning images of MOS loaded-Cd(II)

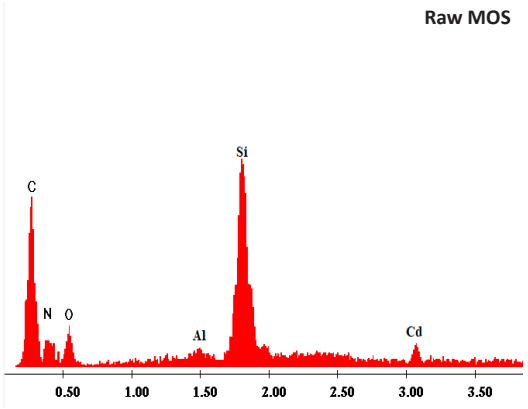

Fig. 4a. EDX scanning images of raw MOS

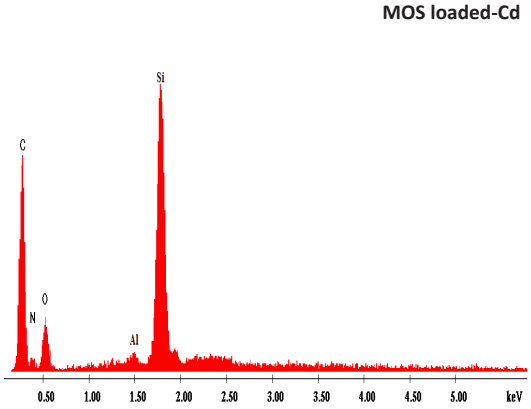

Fig. 4b. EDX scanning images of MOS loaded-Pb(II)

Raw MOS

Element	Wt %	At %	K-Ratio
C K	59.31	65.57	0.3586
N K	12.95	12.27	0.0138
O K	26.34	21.86	0.0353
Si K	1.01	0.08	0.0192
Al K	0.4	0.22	0.0151

MOS loaded-Cd

Element	Wt %	At %	K-Ratio
C K	60.19	66.11	0.3754
N K	16.11	15.18	0.0170
O K	22.36	18.43	0.0282
Cd K	0.34	0.28	0.0116
Si K	0.85	0.08	0.0082
Al K	0.15	0.01	0.0071

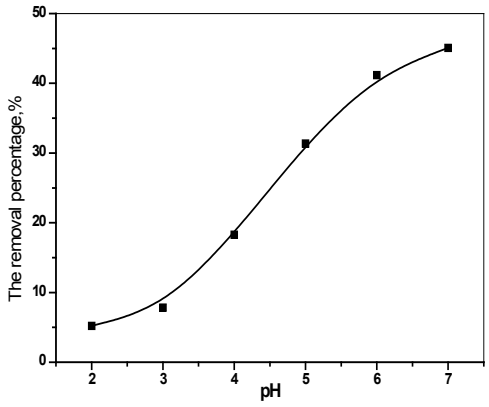

Fig. 5. Effect of the solution pH on the removal percentage of Cd(II).

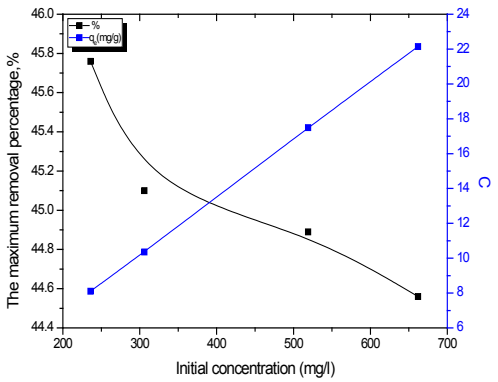

Fig. 6. Effect of the initial Cd(II) on the maximum % and uptake (mg/g)Cd.

Cd (II) concentrations can provide a driving force to overcome the mass transfer resistance of the adsorbate. Inbaraj and Sulochana [41] observed a similar trend and suggested that this effect is caused by an increase in the driving force offered by concentration gradient at higher adsorbate concentrations. Moreover, with the increase of initial Cd (II) concentration, the percent removal of the adsorbate decreases because of the presence of more Cd(II) ions and limited adsorption sites on the adsorbent materials. The above discussion suggests that the adsorption process is highly dependent on initial concentration.

Effect of the solution pH

Effect of pH variation on the %adsorption was carried out by varying the pH in a range of 2.0–7.0. The % adsorption of Cd (II) ions there was a slow increase in adsorption process with increasing pH values from 2 to 3.0 i.e. 5.22%–7.84% (Fig. 6). As the pH was raised from 3–6.0, there was a sharp increase in adsorption process i.e. 7.84%–41.17%. Further increase in the pH

(pH > 6.0) resulted in slow increase in adsorption process (from 41.17 to 45.1%). This behaviour can be explained by the surface charge of the adsorbent, MOS, which was determined by the salt addition method. This method affirmed that pH_{pzc} of the MOS was 6.9. Meaning thereby that the surface of MOS is positively charged at pH < 6.9 and acquired to some extent negative charge and attracts Cd^{2+} ions with increasing pH values. Thus at pH 2.0, adsorption of Cd(II) ions was low as the surface of MOS and Cd(II) ions have positive charge. This means functional groups (hydroxyl, carboxylic, ester, alcoholic, carbonyl and acetyl) or binding sites gets protonated which in turn compete with the adsorbate ions and inhibits binding of Cd (II) ions with MOS through ionic repulsions. As the pH value raised from 6 to 7, slow increase in adsorption was observed because of the formation of soluble $Cd(OH)_2$ species with already existing $CdOH^+$ species, suggesting that at pH > 6 hydrogen bonding governs the adsorption process and not electrostatic attractions as at comparatively lower pH values [42]. Hence, the optimum initial pH value for adsorption of Cd^{2+} ions from aqueous solution by MOS was determined as 7 ± 0.1, which was maintained in the further experimental studies.

Effect of the contact time

The biosorption efficiency of Cd (II) ions on MOS increase along contact time, as is expected, and takes place in two stages (Fig. 7). The first stage in which more than 28.1% of Cd (II) retained was achieved within 30 min and is followed by a slower second stage which reaches equilibrium 45.1% attained in 240 min. These two stages of biosorption can be explained by considering that the number of active sites from biosorbent surface is finite and that the retention of metal ions from aqueous solution occurs gradually. Thus, in the first stage, when the availability of biosorbent surface is higher, the retention of Cd(II) ions involves the external sites and consequently required time is higher.

With the gradual occupation of binding sites, the Cd (II) uptake process requires the penetration of the inner active sites, making the biosorption process to become slower. The significantly lower contact time for the biosorption process is an important advantage of using MOS in heavy metals removal, especially in continuous systems. The low value of contact time necessary to reach the equilibrium state sustain the hypothesis that biosorption of Cd(II) onto MOS is probably, controlled by electrostatic (ion exchange) interactions between positive metal ions and negative charged functional groups from the biosorbent surface [43].

Adsorption isotherm

Adsorption isotherm is a relationship describes the adsorbate distribution between the adsorbent surface and the solution when adsorption equilibrium is reached at a constant temperature. It is significantly important for adsorption system, for it can be used to compare the properties with different adsorbents quantitatively, elucidate the adsorption state of adsorbate on adsorbent surface and calculate adsorption parameters such as theoretical adsorption capacity, and adsorption heat. Thus, adsorption isotherm usually provides some insight in sorption mechanism, surface

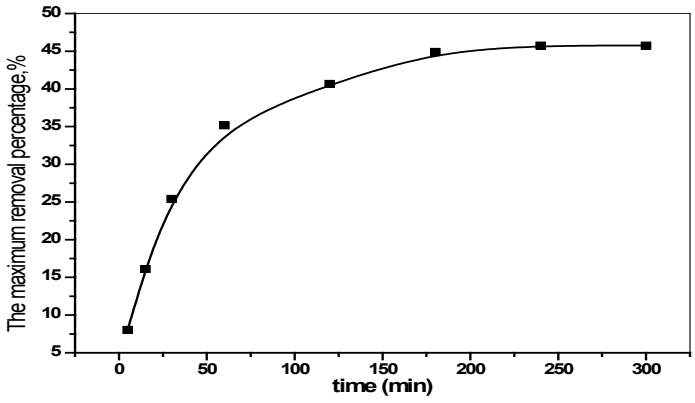

Fig. 7. Effect of the agitation time on the Cd (II) uptake

properties and affinity of adsorbent.

The results of adsorption equilibrium of Cd(II) on MOS biomass at 298 K are given in Fig. 8a,b. The equilibrium data are fitted by four isotherm models named Langmuir, Freundlich, Dubinin–Radushkevich (D–R) and Temkin, respectively. The validity of isotherm models used in this study is assessed by correlation coefficient (R^2). For different isotherm models, a high correlation coefficient represents a good regression. A correlation coefficient can be obtained from the Origin 8.0 software.

The fitted results of all isotherm models investigated in this study are presented in Table 1, and the predicted curves by four isotherm models mentioned above are also depicted in Fig. 8a,b. Compared with Langmiur, Temkin, and D–R isotherm models which give lower correlation coefficients with the values of 0.76181, 0.97802 and 0.9073, respectively, the highest regression correlation coefficients (0.99965) is observed for Freundlich model in Table 1. Accordingly, the adsorption of Cd(II) on MOS can be well described by the Freundich isotherm model. The Freundlich isotherm model allows for several kinds of adsorption sites on the solid surface and represents properly the adsorption data at low and intermediate concentrations on heterogeneous surfaces. In this study, the Cd (II) concentration ranges from 236–662 ppm, being consistent with the assumption of Freundlich model. Furthermore, the MOS is a kind of macro-porous material, which indicates the surface of MOS is heterogeneous. The photos obtained from Scanning Electron Microscope also show that the surface of MOS is heterogeneous. These are the reasons why the Freundlich model can well describe the adsorption equilibrium data of Cd (II) on MOS. The value of n, one of Freundlich constants, relates to the surface heterogeneity of adsorbent, giving an indication of how favorable an adsorption process. When $0 < 1/n < 1$, the adsorption is favorable; $1/n = 1$, the adsorption is homogeneous and there is no interaction among the adsorbed species; $1/n > 1$, the adsorption is unfavorable [43]. As can be noticed in our study, the value of $1/n$ is 0.959, and ranges from 0 to 1, showing that the adsorption of Cd (II) on MOS is favorable.

The predicted curves by different isotherm models in Fig. 8a,b also show that Freundlich model give satisfactory fits to the equilibrium adsorption data of Cd (II) on Moringaoleifera seed, compared to other isotherm models investigated in this study[43].

Separation factor (R_L)

A dimensionless constant, separation factor (R_L) can be used to predict whether a sorption system is favorable or unfavorable in batch adsorption process. R_L values between 0 and 1 represent the favorable isotherm. R_L was calculated from Langmuir isotherm based equation. The separation factor (R_L) profile of adsorption of Cd(II) on seed of *moringa oleifera* is presented in Fig. 9. The parameter, R_L, indicates the shape of the isotherm and the nature of the sorption process as given: $R_L > 1$ = unfavorable isotherm, $R_L = 1$ = linear isotherm, $R_L = 0$ = irreversible isotherm, $0 < R_L < 1$ = favorable isotherm. The values of R_L for Cd(II) were calculated and plotted against initial metal ion concentration. Favorable isotherm (Fig. 9) showed that, the sorption of Cd (II) on the seed biomass of *moringa oleifera*

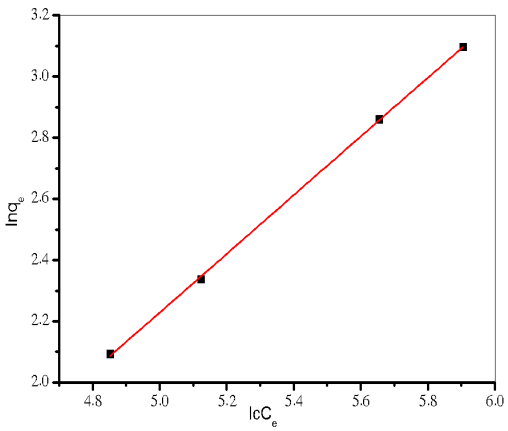

Fig. 8a. Freundlich plot of Cd(II) adsorption.

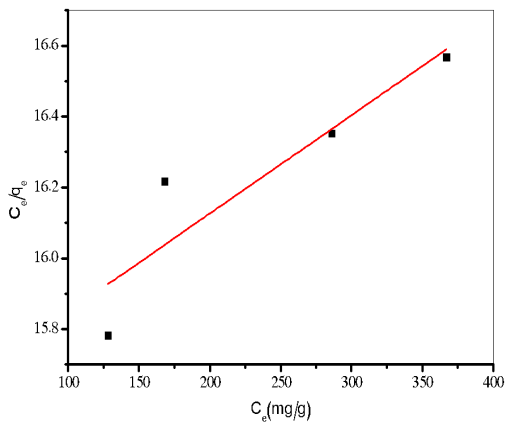

Fig. 8b. Langmuir plot of Cd(II) adsorption.

decreased as the initial metal ion concentration increased from 236 to 662 ppm, indicating that adsorption is even favorable for the higher initial metal ion concentrations. The sorption process was favorable for Cd (II) removal at all concentrations investigated. From the figure it can be noted that adsorption process is favorable on low as well as high concentrations [44].

Surface coverage (θ)

The fraction of biomass surface covered by Cd(II) was studied using Langmuir type equation. By plotting the surface coverage value (θ) against Cd(II) concentration (Fig. 10)[45].

$$\Theta = K_L C_o (1 - \theta) \text{ ----------} \quad (5)$$

Where K_L is the Langmuir adsorption coefficient, θ the surface coverage. and C_o is the initial concentration of Cd(II).

The increase in initial Cd (II) concentration from 236 to 662 ppm for MOS biomass increases the surface coverage on the biomass until the surface is nearly fully covered with a monolayer (Fig. 10). At all concentrations, the metal adsorption rate on biomass surface becomes dependent on the Cd (II) concentration.

On the other hand, the A_T and B_T parameters of the Temkin equation were calculated (Fig. 11) for Cd (II) ions adsorption (Table 1). It was obtained that the value of R^2 for Temkin model (0.97802) is higher than calculated for the Langmuir and D-R model (0.76181 and 0.9073, respectively). The data of equilibrium isotherms for the system Cd (II) /MOS may be described also by the Temkin model as it can be observed. In addition, the heat of sorption process, estimated by the Temkin isotherm model is 13.3 J/Mol.

However, the Dubinin–Radushkevich isotherm model (D-R) assumes a fixed volume or 'sorption space' close to the sorbent surface and determines the heterogeneity of sorption energies within the sorption space and is applied in the linearized form. The plot of ln q_e versus ε^2 (Fig. 12) yield coefficients of determinations and the result of X_m (22.79 mg/g) computed from the slope and intercept of respective plots are documented (Table 1). R^2 values (0.9073) showed that the D–R model was relatively poor fit to the experimental data of Cd (II) adsorption. The mean free energy of sorption (E_{D-R}) can be defined as the free energy change when one mole of ion is transferred from infinity in solution to the sorbent. The E_{D-R} value of this study shows a high value (0.0129 kJ mol^{-1}), indicating the physical nature of the Cd (II) adsorption processes onto the resin.

Thermodynamic parameters

Table 4 shows the thermodynamic parameters ($\Delta G°$, $\Delta H°$, and $\Delta S°$) obtained for the metal ions adsorption on MOS adsorbent. The K_d values was employed in calculating the thermodynamic parameters (Fig. 13). It was observed that the values of enthalpy changes, $\Delta H°$, were positive for Cd (II) adsorption on MOS. The positive values imply that the reactions were endothermic; hence, increased solution temperature would result in increased uptake of aqueous metal ions [46]. However, the functional groups on the biomass surface tend to reduce, significantly, the energy requirement for the adsorption process. This is seen in the decrease in the enthalpy of the adsorption reaction. However, the $\Delta G°$ values indicated that the adsorption processes were non-spontaneous and not feasible. The $\Delta S°$ values of the adsorptions were positive for Cd(II)

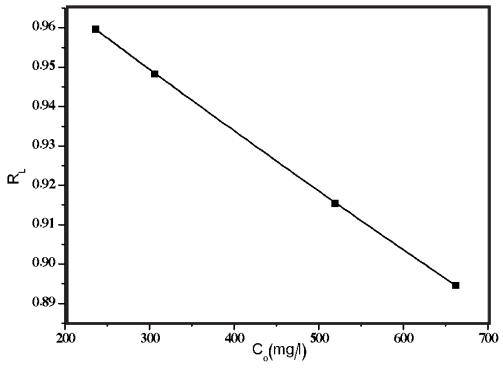

Fig. 9. Separation factor profile.

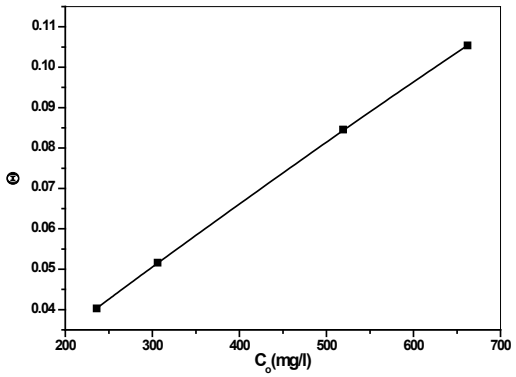

Fig. 10. A plot of surface coverage.

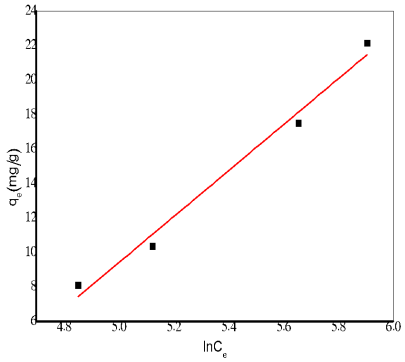

Fig. 11. The Temkin plot of Cd(II) adsorption.

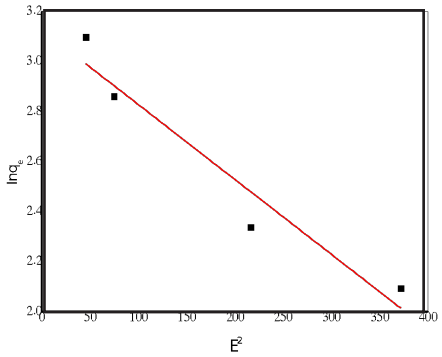

Fig. 12. The D-R plot of Cd(II) adsorption.

TABLE 1. Isotherm parameters.

Freundlich				Langmuir			
1/n	K_f (mg/g)	R^2	Q_{max} (mg/g)	K_L (L/mg)	C_o mg/l	R_L	R^2
0.959	0.0765	0.99965	357.14	0.000179	236	0.959	0.79181
					306	0.948	
					519	0.915	
					662	0.894	
D-R				Temkin			
B (mol^2/kJ^2)	q_{D-R} (mg/g)	E(kJ/mol)	R^2	A_T (L/min)		B_T	R^2
0.00299	22.79	0.0129	0.9073	0.0136		13.3	0.97802

adsorption on MOS. This is an indication of increase in randomness of the Cd (II) ions at the solid–liquid interface as the adsorption processes preceded towards equilibrium [47].

The sticking probability, S*, is a function of the adsorbate/adsorbent system under consideration and dependent on the temperature of the system. The parameter S* indicates the measure of the potential of an adsorbate to remain on the adsorbent indefinitely. (Table 2). The effect of temperature on the sticking probability was evaluated throughout the temperature range from 277 to 323 K by calculating the surface coverage at the various temperatures (Fig. 14). Table 2 also indicated that the values of $S^* \leq 1$ (0.00577) for the MOS, hence the sticking probability of the Cd (II) ion onto the two adsorbent systems are very high [20].

Sorption activation energy

According to Arrhenius equation, activation energy of the adsorption (E_a, kJ mol^{-1}) can be calculated using the above equation. The magnitude of activation energy gives an idea about the type of adsorption which is mainly physical or chemical. Low activation energies (<40 kJ mol^{-1}) are characteristics for physical adsorption, while higher activation energies (>40 kJ mol^{-1}) suggest chemical adsorption [48]. According to activation energy obtained for the adsorption of Cd (II) onto the MOS was 11.6 kJ mol^{-1} indicates that the adsorption process is physio-sorption. The low value of E_a suggests that the energetic barrier against the adsorption of metal ion is easy to overcome; therefore, adsorption process occurs rapidly [49].

Coagulation Study

Effect of the solution pH on the coagulation process

In order to investigate the coagulation behavior

of Cd (II) ions on MOS, the effect of solution pH on Cd (II) coagulation was carried out initial Cd (II) concentration of 306 ppm and 25^{0}C. As shown in Fig. 15, one can see that the removal percentage of Cd (II) increased quickly from ~88.61% to ~91.80% with the pH increased from ~2 to ~4, then decreased from ~91.80% to ~93.13% with the solution pH increasing from ~4 to ~6, and then increased from ~90.18% to ~93.54% with the solution pH increasing from ~6 to ~7. With the change of acid-degree, the coagulation changes a little and maintains at a high level, which may be attributed to weakly protonation effect and thereby increases the electrostatic attraction. In general, the surface property of coagulant is affected by solution pH distinctly. In addition, the pH_{pzc} of MOS as a function of pH were shown in Fig. 15. It is clear that the pH_{pzc} value of MOS was positive at $2 < pH < 6.7$. Thus, one can conclude that the high removal percentage at neutral pH is attributed to the electrostatic attraction between the Cd (II) negatively charged complexes and positively charged MOS. At strongly acidic condition, the high concentration of H^+ changes the existing form of oxygen-containing functional

TABLE 2. Thermodynamic parameters.

Temp. (K)	ΔG^0 KJ/Mol	ΔH^0 KJ/Mol	ΔS^0 J/mol K	S*	Ea KJ/Mol
277	15.9				
298	6.9	66.2	188.4	0.00577	11.6
313	5.95				
328	6.77				

TABLE 3. Isotherm parameters-Coagulation-Cd.

Freundlich			Langmuir			
1/n	K_f (mg/g)	R^2	Q_{max} (mg/g)	K_L (L/mg)	R_L	R^2
1.46	1.37	0.91137	200.8	0.0114	0.270 0.222 0.144	0.4800

D-R				Temkin	
B (mol^2/kJ^2)	qD-R (mg/g)	E(kJ/mol)	R^2	KT (L/min)	R^2
0.0000832	193.1	0.0775	0.75078	0.07	0.8236

TABLE 4 .Thermodynamic parameters-Coagulation-Cd.

Temp. (K)	ΔG^0 KJ/Mol	ΔH^0 KJ/Mol	ΔS^0 J/mol K	S*	Ea KJ/Mol
277	-3.7				
298	-2.79	-10.6	-25.2	4.3	-9.9
313	-2.94				

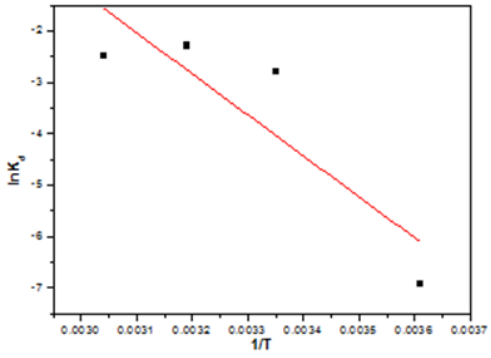

Fig. 13. Van,t Hoff plot of Cd(II) adsorption.

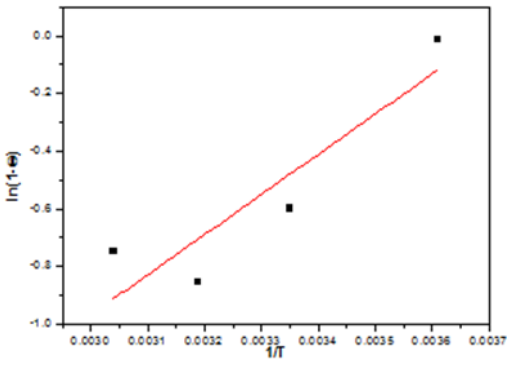

Fig. 14. Sticking probability plot of Cd(II) adsorption

groups due to protonation reactions, such as the -OH group of MOS changes to $-OH_2^+$ and the main group of MOS presents as -COOH, which weakens the hydrogen bond, leading to the low removal percentage [50]. At near pH_{pzc} value, the adsorbent surface charge changes less positive [51].

Effect of the temperature

In order to further investigate the Cd (II) coagulation, the Cd (II) coagualtion on MOS as a function of solution temperature was carried out. One can clearly see that solution temperature effects greatly on Cd (II) coagulation from (Fig. 16). The percentage of Cd (II) coagulation on MOS decreases from 94.5% to 93.13% with temperature increasing from 4 °C to 25 °C, On the other hand, in the temperature range of 25–40 °C, the coagulation percentage of Cd (II) was relatively increased with the increase of temperature to reach 93.17 %, suggesting that the coagulation process of Cd (II) to the MOS surfaces needs energy [52]. However, the coagulation percentage keeps unchanged at T > 40 °C, which is attributed to the strong Brownian motion [53]. With the increase of temperature, kinetic energy of Cd (II) ions increases and the it becomes unstable, which is unfavorable for the stability and chemical bonding between Cd (II) and MOS surfaces [54]. A similar result was obtained by Wen et al., 2017 [55].

Determination of the time-concentration profiles of Cd (II) removal

The time concentration profiles (24, 48 and 72 min) of the Cd (II) removal from the synthetic contaminated water were monitored at different initial Cd (II) concentration that varied between 236, 306 and 519 ppm at the optimum coagulant dosage obtained (i.e. 0.1665 mg). The results obtained (Fig. 17) from this study showed that the initial concentration greatly influenced the values of the coagulation efficiencies obtained. The shapes of the curves which depicted the attainment of the optimum removal percentage time was 24 h with the initial Cd (II) cadmium concentration of 236 ppm, while the values of the coagulation efficiencies obtained, at the other different initial Cd (II) concentrations, showed decrease very sharp with increases of the initial Cd (II) concentrations. Furthermore, the values of the coagulation efficiencies (%) were higher at lower initial cadm ium Cd (II) concentrations than at higher initial Cd (II) concentrations. The high dependency of the values of the coagulation efficiency of the MOS on the initial Cd (II) concentrations attributed to the fact that as the removal value decreases there is increasing concentrations of the colloidal particulates that inhibited coagulation (i.e. the Cd (II) ions) in the aqua matrix.

Coagulation mechanism

Coagulants change the surface charge properties of solids to allow the agglomeration or enmeshment of particles into a flocculated precipitate. The coagulation and the flocculation of suspended particles and colloids result from different mechanisms including electrostatic attraction (reduction of the repulsive potential of electrical double layers of colloids), sorption (related to protonated amine groups), bridging (related to polymer high molecular weight). In some cases, the amount of protonated amine groups added to the solution is far below the number of charges necessary for the neutralization of the anionic charges held by the colloids; the removal of particles can be explained in this case

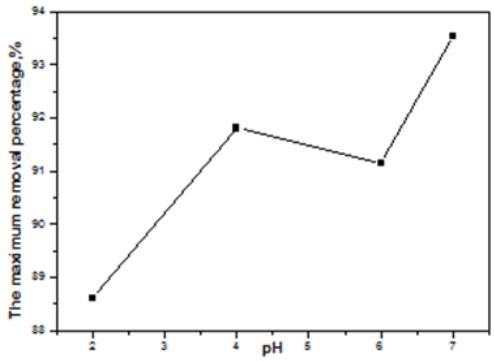

Fig. 15. Effect of the solution pH.

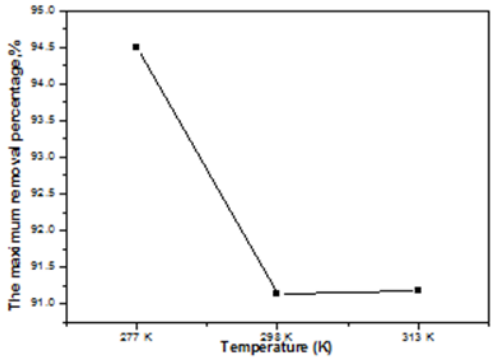

Fig. 16. Effect of the temperature.

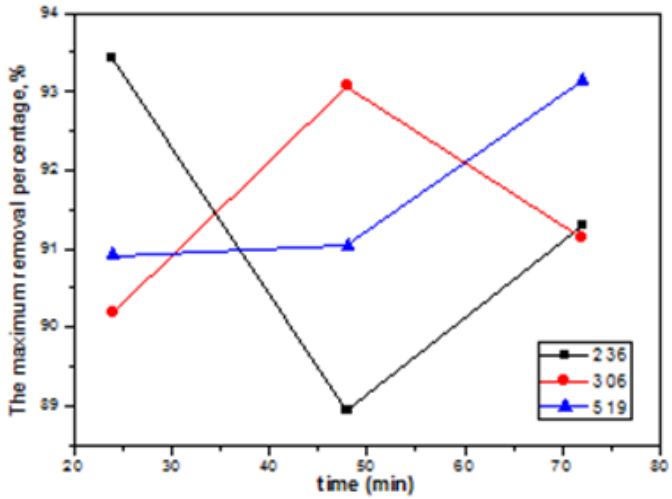

Fig. 17. The time-concentration profiles of the removal of Cd (II) at varying initial Cd (II) concentration using Coagulation technique

by a combination of distinct mechanisms such as electrostatic patch and bridging [56-58].

The isotherm models

The isotherm plots (Figs not shown) whereas the equilibrium parameters are presented in Table 3. Based on the R^2 values, the coagulation process was best described by the Freundlich model (0.91137), followed by Langmuir (0.4800), Temkin (0.8236) and D-R (0.75078). According to the Freundlich model, a multi-layer of Cd (II) ions were adsorbed onto the heterogeneous surface of MOS and these binding sites were associated with different coagulation energies. It was further assumed that the stronger binding sites of MOS were first occupied. The process unfavorably is related to the Freundlich exponent, *1/n*. The coagulation would be favorable if $0 < 1/n < 1$. As observed from Table 3, Cd (II) was unfavorably removed by MOS as *1/n* values was >1.

Adsorption thermodynamics

The process spontaneity and feasibility were evaluated based on thermodynamic parameters such as the Gibbs free energy change (ΔG), entropy change (ΔS), and enthalpy change (ΔH), and the results are summarized in Table 4 (Fig not shown). The value of ΔG was found to be negative for all temperatures. The results confirmed that the removal of Cd (II) by MOS was thermodynamically feasible and spontaneous. Nevertheless, the coagulation process was exothermic as supported by the negative value of ΔH. The ΔH value was -10.6KJ/Mol, suggesting that the nature of process was physio-sorption [59]. The negative ΔS value corresponded to a decrease in

randomness at the solid-liquid interface when Cd (II) was coagulated onto MOS.

The parameter S* indicates the measure of the potential of coagulation to remain on the MOS indefinitely. It can be expressed as in Table 4 (figure not shown). The effect of temperature on the sticking probability was evaluated throughout the temperature range from 277 to 323 K by calculating the surface coverage at the various temperatures. Table 4 also indicated that the values of S*>1 (4.3) for the MOS, hence the sticking probability of the Cd (II) ion onto the adsorbent system are very low [20].

Sorption activation energy

According to Arrhenius equation, activation energy of the adsorption (E_a, kJ mol^{-1}) can be calculated using the above equation. The magnitude of activation energy gives an idea about the type of adsorption which is mainly physical or chemical. Low activation energies (<40 kJ mol^{-1}) are characteristics for physical process, while higher activation energies (>40 kJ mol^{-1}) suggest chemical adsorption [48]. According to activation energy obtained for the coagulation of Cd (II) onto the MOS was -9.9kJ mol^{-1} indicates has no obvious physical significance, the adsorption studies of this should be performed at much more lower solution temperatures to obtain adsorption activation energy[49].

Comparative efficiency of Moring Oleifera seeds toward Cd (II) removal

Herein, biomaterial of *Moring Oleifera seeds* (MOS) as biosorbent and coagulant was recommended for the removal of Cd ions in environmental samples. The structural, chemical and morphological analysis demonstrates that the MOS exhibits low structural defects and villous morphology with submicron sized pores.

This work highlights new insight into the adsorption and coagulation properties of MOS, which can pave the way for its application for wastewater treatment in environmental pollution cleanup as follow:

(1) In the coagulation process, the removal percentage of Cd (II) is higher than of adsorption process at the same concentrations, because an increase of some coagulant sits in MOS as coagulant more than of MOS as adsorbent (Fig. 18).

(2) In the coagulation process, the removal percentage of Cd (II) is higher than of adsorption process at the same solution pHs values. In general, the removal percentage of Cd (II) shows an increase with increases of the pH values. However, increases of the removal percentage of Cd (II) in adsorption process shows high gradual increases while in coagulation process shows a low gradual an increases with increases of the pH values (Fig. 19).

(3) In the coagulation process, the removal percentage of Cd (II) is higher than of adsorption process at the same temperatures (Fig. 20).

(4) In the adsorption process, equilibrium (%) is reached when the contact time is 240 min while in coagulation process the equilibrium (%) is reached when the contact time is 2880 min and then decreases with increasing the contact time (4320 min). However, the removal percentage was higher at the coagulation process than adsorption process at equilibrium times (Fig. 21).

(5) The Freundlich isotherm linear equation was better described the adsorption process and coagulation process of the removal of Cd (II) ions.

(6) Compared with the thermodynamic parameters of Cd (II) removal, such as ΔH^o values indicate adsorption process was endothermic while coagulation process was exothermic, ΔS^o values indicate adsorption process was increased in randomness while coagulation process decrease in randomness, and ΔG^o values for adsorption process were positive values along all temperatures studied (277, 298 and 313^{o}K) these indicate the adsorption process was not feasible and non-spontaneous while coagulation process were negative values these indicate the coagulation process was feasible and spontaneous, According to S* values the adsorption system is very high while the coagulation system is very low. From positive of Ea value indicate that the adsorption process was physical process but from negative value of Ea the coagulation process has no obvious physical significance.

Conclusion

Finally, this study provides fundamental support for selecting an optimum technique in Cd (II) treatment for practical applications, and is important to ensure the sustainable development of mines and environmental protection. Furthermore, our results may be appropriate for water treatment.

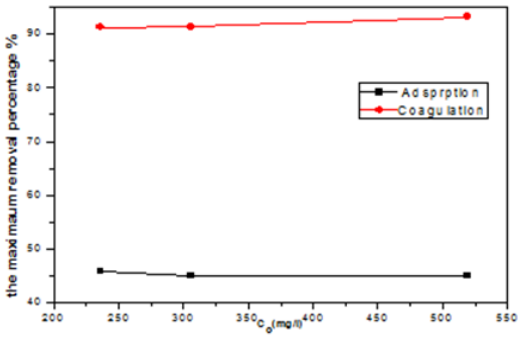

Fig. 18. Comparison of adsorption with coagulation techniques on removal percentage of Cd(II) at different concentrations

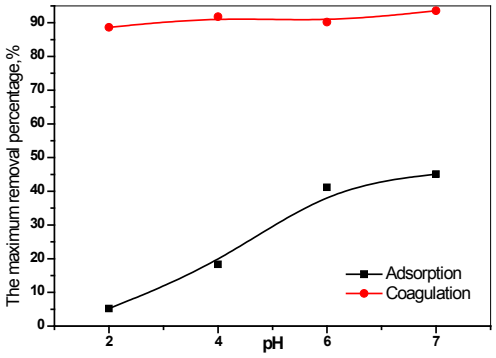

Fig. 19. Comparison between the adsorption and coagulation techniques for removal percentage of Cd(II) at different pHs

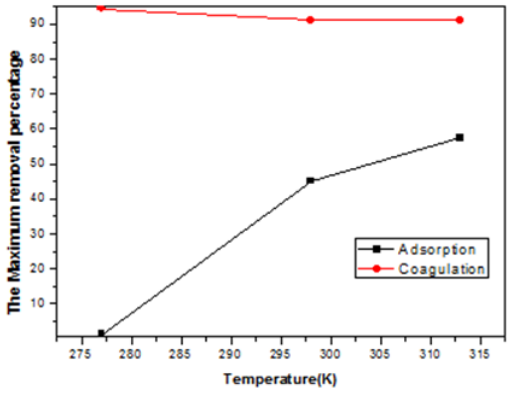

Fig. 20. Effect of the solution temperature on the removal percentage of Cd(II).

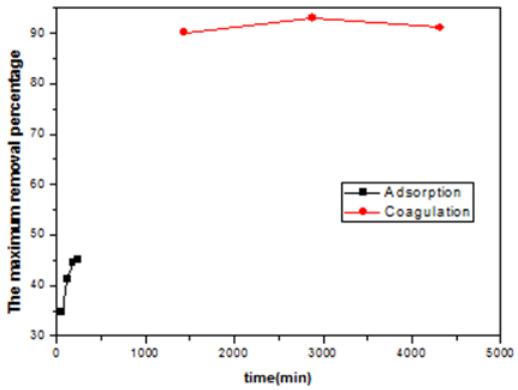

Fig. 21. Comparison between the adsorption and coagulation techniques for removal percentage of Cd(II) at different times

References

1. Ambasht R.S., Ambasht P.K.; *Environment and Pollution: An Ecological Approach* (4th ed.), CBS Publishers & Distributors (2005).

2. Chandrashekhar S. Patil, Datta B. Gunjal, Vaibhav M. Naik, Namdev S. Harale, Anil H. Gore; Waste tea residue as a low cost adsorbent for removal of hydralazine hydrochloride pharmaceutical pollutant from aqueous media: An environmental remediation, *Journal of Cleaner Production,* **206**, 407-418 (2019).

3. Qiang G, Jian X, Xian H.; Recent advances about metal–organic frameworks in the removal of pollutants from wastewater, *Coordination Chemistry Reviews,* **378**, 17-31(2019).

4. Bing Wu; Membrane-based technology in greywater reclamation: A review, *Science of The Total Environment,* **656**, 184-200(2019).

5. Elçin G, Emre D, Yalçın G, Asude H; Characterization and treatment alternatives of industrial container and drum cleaning wastewater: Comparison of Fenton-like process and combined coagulation/oxidation processes, *Separation and Purification Technology,* **209**, 426-433(2019).

6. Bo G., Huan Y., Baoyu G, Hong Y. R., Shuang Z.; *Colloids and Surfaces A: Physicochemical and Engineering Aspects,* **481**, 476-484 (2015).

7. Ying Y. C., Weiying X., Hongjian Z., Dong W., Mengting L.; Comparison of organic matter removals in single-component and bi-component systems using enhanced coagulation and magnetic ion exchange (MIEX) adsorption, *Chemosphere*, **210**, 672-682(2018).

8. Lyu Z., Hongjie Z., Xiaoyu Y.; Preparation and

performance of a novel starch-based inorganic/organic composite coagulant for textile wastewater treatment, *Separation and Purification Technology,* **210**, 93-998 (2019).

9. Maya K., Souad D., Manelle R., Nadjib D., Hakim L.; Valorization of orange industry residues to form a natural coagulant and adsorbent, *Journal of Industrial and Engineering Chemistry,* **64**, 292-299 (2018).

10. Camacho F.P., Sousa V.S., Bergamasco R., Teixeira M.R.; The use of Moringa oleifera as a natural coagulant in surface water treatment, *Chemical Engineering Journal,* **313**, 226-237 (2017).

11. Ndabigengesere A., Narasiah K.S.; Quality of water treated by coagulation using Moringa oleifera seeds, *Water Research,* **32**, 781-791(1998).

12. Dey B.K., Hashim M.A., Hasan S., Gupta B.S.; *Advnced Enviromental. Research.* **8**, 455-466 (2004).

13. Vieira A.M.S., Vieira M.F., Silva G.F., Araújo ÁA., Fagundes M.R.K, M.T., Veit R.; Combined water treatment with extract of natural Moringa oleifera Lam and synthetic coagulant. *Water Air Soil Pollut.,* **206**, 273-281(2010).

14. Arnoldsson E., Bergam M., Matsinhe N., K.M.; J. Assessment of drinking water treatment using Moringa Oleifera natural coagulant. *Water Manag. Res.,* **64**, 137-150 (2008).

15. Nand V., Koshy K., Maata M., Sotheeswaran S.; Water Purification using Moringa oleifera and Other Locally Available Seeds in Fiji for Heavy Metal Removal. *Int. J. Appl. Sci. Technol.,* **2**, 125-129 (2012).

16. Freundlich H.; Zeit schrift für Physikalische. *Chemie* **57**, 384-470 (1906).

17. Langmuir I.; The adsorption of gases on plane surfaces of glass, mica and platinum. *J.Am. Chem. Soc.* **57**, 1361-1403(1918).

18. Temkin I.M., V. Pyzhev; *Acta Physiochem. SSR,* **12**, 217-222 (1940).

19. Dubinin, M.M., L.V. Radushkevich; *Chemisches Zentralblatt*, **1**, 875-890 (1947).

20. Singh, B., Das, S. K., Adsorptive removal of Cu(II) from aqueous solution and industrial effluent using natural/agricultural wastes, *Colloids and Surf. B: Biointer.* **107**, 97– 106 (2013).

21. Araújo C.S.T., Alves V.N., Rezende H.C., Almeida L.S., R.M.N. De A., César R., Tarley T., Segatelli M.G., Coelho N.M.M.; Potential of M. oleifera for the treatment of water and wastewater. *Water Sci. Technol.,* **62**, 2198-2203 (2010).

22. Kwaambwa H.M., Maikokera R.; Infrared and circular dichroism spectroscopic characterisation of secondary structure components of a water treatment coagulant protein extracted from Moringa oleifera seeds, *Colloid Surf. B,* **64**, 118-125 (2008).

23. Ningchuan F, Xueyi G, Sha L; Adsorption study of copper (II) by chemically modified orange peel, *Journal of Hazardous Materials,* **164**, 1286–1292 (2009).

24. Muqaddas T, Arjumand I. D., Umar F., Madiha T.; Efficacy of spent black tea for the removal of nitrobenzene from aqueous media, *Journal of Environmental Management,* **223**, 771-778 (2018).

25. Shalini T., Ahin R., Sajitha N., Smeer D, Roopa R.; Removal of U(VI) from aqueous solution by adsorption onto synthesized silica and zinc silicate nanotubes: Equilibrium and kinetic aspects with application to real samples, *Environmental Nanotechnology, Monitoring & Management,* **10**, 127-139 (2018).

26. Aline T.A., Mariana O. S., Raquel G. G., Rosângela B, Marcelo F. V., Angélica M. S. V.; Protein fractionation of seeds of Moringa oleifera lam and its application in superficial water treatment, *Separation and Purification Technology,* **180**, 114-124 (2017).

27. Temesgen G. K., Alemayehu A. M., Simiso D., Thabo T.I.N., Mathew M. N.; Study on adsorption of some common metal ions present in industrial effluents by Moringa stenopetala seed powder, *Journal of Environmental Chemical Engineering,* **6**, 1378-1389 (2018).

28. Aline T. A. B., Mariana O. S., Raquel G. G., Rosângela B., Marcelo F. V., Angélica M. S. V.; Protein fractionation of seeds of Moringa oleifera lam and its application in superficial water treatment, *Separation and Purification Technology,* **180**, 114-124 (2017).

29. Jayaram K., Prasad M. N. V.; Removal of Pb(II) from aqueous solution by seed powder of Prosopis juliflora DC., *Journal of Hazardous Materials,* **169**, 991-997 (2009).

30. Fan S., Wang Y., Wang Z., Tang J., Tang J., Lia

X.; Removal of methylene blue from aqueous solution by sewage sludge-derived biochar: Adsorption kinetics, equilibrium, thermodynamics and mechanism, *J. Environ. Chem. Eng,* **5**, 601-611 (2017).

31. Ahmed M.J., Hameed B.H. ; Adsorption behavior of salicylic acid on biochar as derived from the thermal pyrolysis of barley straws, *Journal of Cleaner Production,* **195**, 1162-1169 (2018).

32. Abdulkarim S.M., Long K., Lai O.M., Muhammad S.K.S., Ghazali H.M.; Some physico-chemical properties of Moringa oleifera seed oil extracted using solvent and aqueous enzymatic methods, *Food Chem.*, **93**, 253-263 (2005).

33. Temesgen G. K., Alemayehu A. M., Simiso D., Thabo T.I.N., Mathew M. N.; Study on adsorption of some common metal ions present in industrial effluents by Moringa stenopetala seed powder, *Journal of Environmental Chemical Engineering,* **6**, 1378-1389 (2018).

34. Araujo C.S.T., Carvalho D.C., Rezende H.C., Almeida I.L.S., Coelho L.M., Coelho N.M.M., Marques T.L., Alves V.N.; Bioremediation of Waters Contaminated with Heavy Metals Using Moringa oleifera Seeds as Biosorbent, *Appl. Bioremediat. Act. Passiv.Approaches.InTech,* **406** (2013).

35. Isabela M. R., Rebecca M. P., Rosangela B., Marcelo F. V., Angélica M. S. V.; Removal of tartrazine from aqueous solutions using adsorbents based on activated carbon and Moringa oleifera seeds, *Journal of Cleaner Production,* **171**, 85-97(2018).

36. Gan M., Song Z., Jie S., Zhu J., Zhu Y., Liu X.; Biosynthesis of bifunctional iron oxyhydrosulfate by Acidithiobacillus ferroxidans and their application to coagulation and adsorption, *Materials Science and Engineering: C,* **59**, 990-997 (2016).

37. Mateus G. A. P., Paludo M.P., Santos T. R. T., Silva M. F., R. Bergamasco; Obtaining drinking water using a magnetic coagulant composed of magnetite nanoparticles functionalized with Moringa oleiferaseed extract, *Journal of Environmental Chemical Engineering,* **6**, 4084-4092(2018).

38. Kebede T. G., Dube S., Mengistie A. A., Nkambule T. T.I., Nindi M. M.; Moringa stenopetala bark: A novel green adsorbent for the removal of metal ions from industrial effluents, *Physics and Chemistry of the Earth Parts A/B/C,***107**,45-57 (2018).

39. Nwaiwu N.E., Zalkiful M.A., Raufu I.A.; *J. Appl. Phytotechnol. Environ. Sanit.*, **1**, 1-9 (2012).

40. Sunita R., Bhagat R., Dharamender K., Ghansh Y. S. C., Veena J.; Functionalization of Moringa oleifera gum for use as Hg2+ ions adsorbent, *Journal of Environmental Chemical Engineering,* **6**, 1805-1813 (2018).

41. Inbaraj B.S., Sulochana N.; Mercury adsorption on a carbon sorbent derived from fruit shell of Terminalia catappa. *J. Hazard.Mater.,* **133**, 283-290 (2006).

42. Sunita R., Bhagat R., Dharamender K., Ghansh Y. S. C., Veena J.; Functionalization of Moringa oleifera gum for use as Hg2+ ions adsorbent, *Journal of Environmental Chemical Engineering,* **6**, 1805-1813 (2018).

43. Ahmad B.A., Maurice N.C., Mu N., Saeed S., Gavin W., Mangwandi C. ; Activated lignin-chitosan extruded blends for efficient adsorption of methylene blue, *Chemical Engineering Journal*, **307**, 264-272 (2017).

44. Muhammad A. H., Raziya N., Haq N. B., Najum R. A., Tariq M. A.; Ni(II) biosorption by Cassia fistula (Golden Shower) biomass, *Journal of Hazardous Materials,***139**, 345-355 (2007).

45. Diagboya P.N., Olu O. B.I., Adebowalev K.O.; Distribution and interactions of pentachlorophenol in soils: The roles of soil iron oxides and organic matter, *J. Contam.Hydrol.,* **191**, 99-106 (2016).

46. Bamidele I. Olu O., Paul N. D., Emmanuel I. U., Alimoh H. A., Rolf A. D., Kayode O.A.; Fractal-like concepts for evaluation of toxic metals adsorption efficiency of feldspar-biomass composites, *Journal of Cleaner Production,* **171**, 884-891 (2018).

47. Anirudhan T.S., Radhakrishnan P.G.; Thermodynamics and kinetics of adsorption of Cu (II) from aqueous solutions onto a new cation exchanger derived from tamarind fruit shell, *J. Chem. Thermody.,* **40**, 702–709 (2008).

48. Aksu Z. and Tezer S.; Biosorption of reactive dyes on the green alga Chlorella vulgaris, *Process Biochem* **40**, 1347-1361 (2005).

49. Wu L., Liu L., Gao B., R. Munoz C., Zhang M., Chen H., Zhou Z., Wang H.; Aggregation Kinetics of Graphene Oxides in Aqueous Solutions: Experiments, Mechanisms, and Modeling,

Langmuir, **29**, 15174-15181 (2013).

50. Wang J., Wang X., Tan L., Chen Y., Hayat T., Hu J., Alsaedi A., Ahmad B., Guo W., Wang X.; Performances and mechanisms of Mg/Al and Ca/Al layered double hydroxides for graphene oxide removal from aqueous solution, *Chem. Eng. J.,* **297**, 106-115 (2016).

51. Yu S., Wang X., Zhang R., Yang T., Ai Y., Wen T., Huang W., Hayat T., Alsaedi A., Wang X.; Cement-Induced Coagulation of Aqueous Graphene Oxide with Ultrahigh Capacity and High Rate Behavior, *Sci. Rep.,* **7**, 39625 (2017).

52. Zou Y., Wang X., Chen Z., Yao W., Ai Y., Liu Y., Hayat T., Alsaedi A., Alharbi N.S., Wang X.; Superior coagulation of graphene oxides on nanoscale layered double hydroxides and layered double oxides, *Environ. Pollut.,* **219**, 107-117 (2016).

53. Wang J., Yao W., Gu P., Yu S., Wang X., Du Y., Wang H., Chen Z., Hayat T., Wang X.; Adsorption of 4-n-Nonylphenol and Bisphenol-A on Magnetic Reduced Graphene Oxides: A Combined Experimental and Theoretical Studies, *Cellulose,* **24**, 851-861 (2015).

54. Wen Y., Jian W., Pengyi W., Xiangxue W., Shujun Y., Yidong Z., Jing H., Tasawar H., Ahmed A., Xiangke W.; Synergistic coagulation of GO and secondary adsorption of heavy metal ions on Ca/Al layered double hydroxides, *Environmental Pollution,* **229**, 827-836 (2017).

55. Anu M., Mikko V., Mika S.; Natural organic matter removal by coagulation during drinking water treatment: A review, *Advances in Colloid and Interface Science,***159**, 189-197 (2010).

56. Guibal E. and Roussy J.; Coagulation and flocculation of dye-containing solutions using a biopolymer (Chitosan), *Reactive and Functional Polymers*, **67**(1), 33-42 (2007).

57. Brittany A.N., Todd M.P., Robert D.T.; Comparative coagulation performance study of Moringa oleifera cationic protein fractions with varying water hardness, *Journal of Environmental Chemical Engineering,* **4**, Part A, 4690-4698 (2016).

58. Hiew B.Y.Z., Lee L.Y., Lee X.J., S. Thangalazhy G., Gan S., Lim S.S., Pan G.-T., Yang T.C.-K., Chiu W.S., Khiew P.S.; Eco-friendly synthesis of graphene–chitosan composite hydrogel as efficient adsorbent for Congo red, *Process Saf*

دراسة مقارنة لإزالة أيونات الكادميوم عن طريق تقنيتي الامتزاز والتجلط باستخدام نبات المورينجا

عبـدالسميـــع أحمـد سويـلم[1]، شريف سعيد صالح[2] و أحمد ابراهيم حافظ[1]

[1]قسم الكيمياء الفيزيائية - كلية العلوم - جامعة الأزهر- مصر.

[2]قسم الكيمياء الحيوية – مركز البحوث الزراعيه - مصر.

تم توصيف بذور المورينجا باستخدام X-ray ،(FT-IR) ،pHHzp و (SEM) لمعرفة وتحديد المجموعات الوظيفية بها والتى قد تمكننا من استخدامها كعامل ماز وايضا عامل تخثرلتنقية المياه الملوثة بأيونات الكادميوم. وقد أجريت عدة دراسات للعوامل المؤثرة على كفاءة هذه البذور لاستخلاص ايونات الكادميوم من المحاليل الملوثة اصطناعيا للوصول الى افضل الظروف لازالة هذه الايونات، مثل درجة الحموضة، وزمن التفاعل، وتأثير التركيز الابتدائي للأيونات ودرجة الحرارة. وقد أظهرت النتائج التجريبية زيادة في نسبة الإزالة من Cd)II) باستخدام تقنية الإمتزاز مقارنة مع تقنية التخثر مع زيادة تركيز الكادميوم الابتدائي وزمن التفاعل. ومع ذلك، لوحظ وجود اتجاه معاكس مع زيادة قيم درجة حرارة المحلول ودرجة الحموضة. كما انه وجد ان المعادلة الخطية Freudlich isotherm هى افضل النماذج الايزوثيرمية التى تتماشى وتتفق مع عملية الامتزاز وكذلك عملية التخثر لإزالة أيونات الكادميوم. كما تم الحصول ومقارنة العوامل الثيرموديناميكية ذات العلاقة بإزالة الكادميوم مثل ΔS ،ΔH وΔG، وقد لوحظ سلوكيات متميزة، حيث كانت عملية الامتزاز فقد كانت هذه القيم موجبة عند جميع درجات الحرارة التى درست بينما كانت عملية التخثر ذات قيم سالبة. ووفقاً لقيمة S * ،فإن مدى استبقاء ابونات الكادميم مع بذور المورينجا فى النظام الممتز مرتفع جداً في حين أن نظام التخثر منخفض جداً.